MDPI

Article

Designing Coupling of 2-Dimensional PhotoRecepto-Conversion Scheme (2DPRCS) with Clean Unit System Platform (CUSP)

Akira Ishibashi [1,2,*], Sheng-Fu Liang [1,3], Naoto Kato [1,2], Ziling Zhou [1,2], Tsung-Hao Hsieh [3], Junji Matsuda [4] and Nobuo Sawamura [1]

1   Research Institute for Electronic Science, Hokkaido University, N20W10, Sapporo 001-0020, Hokkaido, Japan
2   Department of Condensed Mater Physics, Graduate School of Science, Hokkaido University, Sapporo 060-0810, Hokkaido, Japan
3   Institute of Medical Informatics, National Cheng Kun University, No.1, University Road, Tainan City 701, Taiwan
4   Hiei-Kensetsu Corporation, Hiragishi, Sapporo 062-0933, Hokkaido, Japan
*   Correspondence: i-akira@es.hokudai.ac.jp; Tel.: +81-11-706-9423

Abstract: There has been so far no energo-environmental system, whose design is considered energy-wise as well as cleanliness-wise, put in practical use despite the fact that those systems would be of huge potential importance as disaster shelters for casualties and/or infectious disease patients, in particular, those of COVID-19. We have designed the energo-environmental system based on the 2-Dimensional PhotoRecepto-Conversion Scheme (2DPRCS) and Clean Unit System Platform (CUSP) technologies. We have demonstrated the energo-environmental system can be as clean as US 209D class 1000 or better, quite handily, in a couple of minutes. As for the solar-cell-based energy generation part, we have shown that the needed electric power could be generated using our original technology of the 2DPRCS by simulations, as the possible first application of casualties' and patients' highly clean rest-space that has monitoring ability of the status of those people including sleep assessment. This energo-environmental clean system would be realized with the implementation of 2DPRCS in the near future.

1. Introduction

When we look upon our history, we notice that the best mode in a certain stage of development/evolution would rather become a major hindrance in the next. The conventional solar cells [1], we believe, are experiencing one example, and the typical clean systems [2] another. On the one hand, the de facto standard of typical solar cells is that the place where electric power generation is made is exactly the same place where photons are harvested, i.e., two functions of the photoreception and the photoelectro-conversion are spatially degenerated. On the other hand, conventionally, a fan-filter unit (FFU) in clean rooms filtrates the air and ventilates the room mechanically. Again, two functions, here, of the filtration and the ventilation, are degenerated spatially at FFU. To proceed one step further, we now know that these energy-related and environmental issues should be considered and improved simultaneously in an interconnected manner. Bearing in mind the COVID-19 pandemic [3] and general health improvement, we discuss how we can successfully design and build a system, as an example of those energo-environmental systems, in which medical treatment could be provided in high cleanliness even in an outdoor environment. For such emergency surgeries or other treatments, a compact outdoor-compatible room named bubble operating theater (BOT) [4], for example, has been proposed. With such a compact clean space, it becomes possible to treat patients or

casualties in the outdoor environment where an outbreak of an infectious disease or accident takes place. In those emergencies, the compact clean systems are required to operate with high cleanliness, hopefully at low power consumption. Since emergency operations are in need even in outdoor environments, it would surely be better if high-efficiency solar cells could be used as a power supply for the systems. Thus, a self-powered highly clean system with low-power-consumption equipment is of much importance because it could be put into operation, for example, for treating COVID-19, emergency surgeries, and various kinds of analyses, including sleep assessment [5].

In conventional solar cells [1], on the other hand, electric power generation is made at the same place as photoreception, i.e., the function of photo-harvesting is spatially degenerated with that of electric power generation. Thus, if the solar cell is put on the surface of the compact clean space set in an outdoor environment, the sunlight is blocked by the solar cell, and part of the electricity has to be wasted by the lighting of the room, which is obviously no desirable situation at all. The more power we try to generate with those solar cells, the wider area of the compact system is covered, and the darker the inside becomes. Thus, we need another approach which can achieve solar power generation on the surface of the room without making the inside too dark. In conventional concentrator systems [6,7], the aforementioned spatial functional degeneracy is, in a sense, lifted off, but these systems inevitably become too bulky because the two parts of primary photoreception and electric power generation are connected three-dimensionally by photons, and it is very hard for the whole system to be installed in metropolitan areas. Thus, it could be quite revolutionary if we could connect those 2 parts, not 3-dimensionally (3D) but 2-dimensionally (2D), because, with the volume ratio of 2D to 3D structures being 0, the system can be put compactly on the surface of the outdoor-compatible clean space or room. Luminescent solar concentrators (LSCs) [8–10] are indeed along the 3D-to-2D photo-manipulation approach, but they are not necessarily good for applications of optical wireless power transmission (OWPT) [11,12]. Here, we are interested in a system that is quite effective not only for sunlight harvesting but also for OWPT so that our new system can be powered by sunlight at normal times and by laser beams from outside when in such an emergency as an electric power loss.

2. Designing Coupling Compact Clean Space with Power Generation Equipment

So how can we make the aforementioned compact clean system be equipped with a highly efficient power generation ability? For that, Figure 1, we believe, would be the target structure, for which we have started designing based on a 2-Dimensional PhotoRecepto-Conversion Scheme (2DPRCS) [13,14] with Clean Unit System Platform (CUSP) [15–17]. In Figure 1, shown on the top left is a planar concentrator solar cell based on 2DPRCS. The solar cell can be embedded, for example, into the surface of BOT [2], as depicted in the top right inset. The side view, or cross-sectional view, is shown in the bottom left of Figure 1. The box denoted by "A" in the top right inset is an air conditioner. In the top view of the 2DPRCS, shown in the middle of Figure 1, the photo-reception part is spatially decoupled from but 2-dimensionally connected to the photo-conversion part located at the edge of the 2D waveguide. The photo-reception part of 2DPRCS is realized by a redirection waveguide (RWG) consisting of a photo-propagation direction converter (PDC) [13,18] and discrete-translational-symmetry waveguide (DTSWG) [19,20], as shown in the cross-sectional view at the bottom of Figure 1. If we were to prepare the compact lean system with conventional clean technologies, a fan-filter unit (FFU) would be needed to ventilate the compact room mechanically. Again, two functions, here of the filtration and the ventilation, are degenerated spatially at FFU. The spatial degeneracy of those functions has been effective. For much further improvement, however, we believe this degeneracy has to be re-examined because making clean systems highly efficient is very important, for example, for enabling mass realization of net zero-energy buildings (NZEBs) [21] based on building-integrated photovoltaics, a key to reducing greenhouse gas emissions. Keeping those in mind, we have been developing CUSP [15–17] with gas exchange membrane (GEM) [22,23] and gas exchange unit (GEU) [24,25], which enables a closed airflow system

in marked contrast to conventional cleanrooms and/or clean booths that are open airflow systems. Since CUSP is a closed air-flow system, it is very effective for fighting against infectious diseases because no airborne viruses can come in from outside nor go out from inside, with the air pressure inside being the same as that outside in the closed air-flow system. Moreover, we have investigated how liberated we would be when the degeneracies are lifted off with 2DPRCS in conventional solar cells as well as with CUSP in clean systems [26], and here in this paper, we are ready to couple those two, i.e., the 2DPRCS and the CUSP.
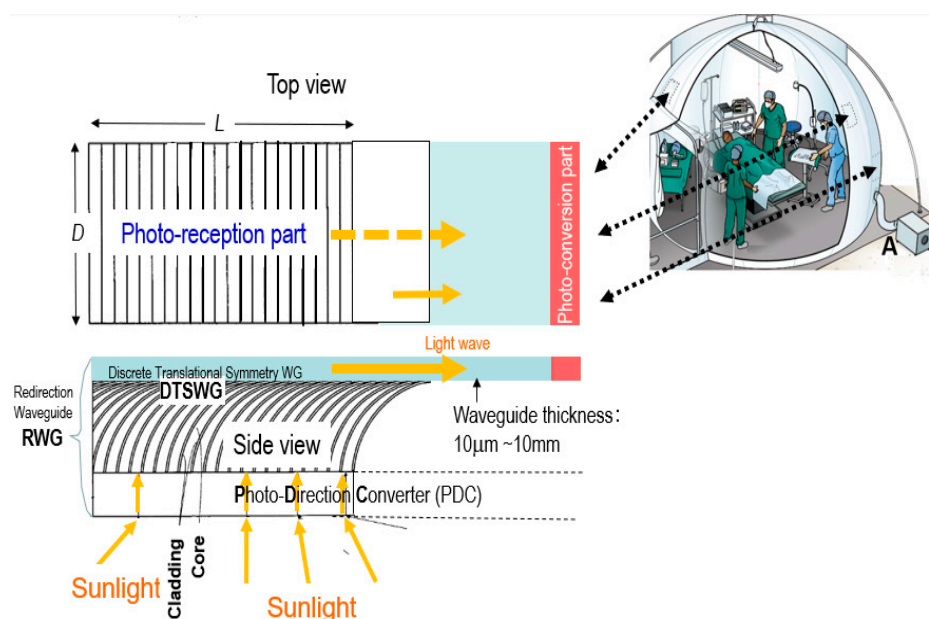

Figure 1. The target structure based on 2-Dimensional PhotoRecepto-Conversion Scheme (2DPRCS) coupled with Clean Unit System Platform (CUSP). The top right inset is an example of a compact clean system called bubble operating theater (BOT) Ref. [2] on which surface, as indicated by thick dotted arrows, we propose to put 2DPRCS-based solar cells as the power supply. In the middle is top view of a planar concentrator solar cell utilizing 2DPRCS. The side view or cross-sectional view is shown bottom left. The box denoted by "A" in the top right inset is air conditioner.

2.1. CUSP Development

2.1.1. Cleanliness in a Handy Jump-Up CUSP

Based upon the CUSP technology developed at Research Institute for Electronic Science (RIES), Hokkaido University, a handy jump-up CUSP (named CAQLEA) that is easy to set up in short time has quite recently been released by Hiei Kensetsu/Eco-earth Corp. [27]. The CAQLEA could be used as the main chamber shown in the top right inset of Figure 1, enjoying its superiority provided by the closed air-flow and gas exchange membrane (GEM) or gas exchange unit (GEU) [25] that consists of stacked multiple GEMs [24]. The CAQLEA is a next generation tent-like CUSP (T-CUSP). The elastic metal bone structure of this self-supporting tent can provide fast installation in 3 s. Then, the ceiling part is attached to the main frame by zipping, and the full system gets ready in a couple of minutes. The top right inset of Figure 2 shows the outlook of the CAQLEA, which is roughly 2 m × 2 m × 1.8 m in size, thus 7.2 m^3 in volume. The CUSP is a closed air-flow system equipped with fan-filter unit (FFU) inside in marked contrast to a conventional clean room, which is an open air-flow system with FFU located at the interface between the inside and outside of the room. Figure 2 shows the time-dependence of densities of particles with diameters of 0.3 μm, 0.5 μm, and 2.0 μm in CAQLEA after the FFU/Air-Purifier is turned on. The flow rate F~1.6 m^3/min and the volume V divided by F is ~4 min., and according to the theoretical analysis [15,17], the particle count n should be e^{-3}~1/20 in 12 min, which is, in fact, in good agreement with the experimental results demonstrated in Figure 3 that demonstrates

cleanliness in the jump-up CUSP (CAQLEA). The number of particles per 1 cubic foot (cf) with diameter of 0.5 μm or larger decreases below 1000/cf in less than 15 min and thus reaches the cleanliness of US FED 209D class 1000 quite rapidly, which is good and appropriate, for example, for treating COVID-19 patients, for sound tight sleep nursing respiratory systems, and for subject's sleep assessment as discussed in the following.
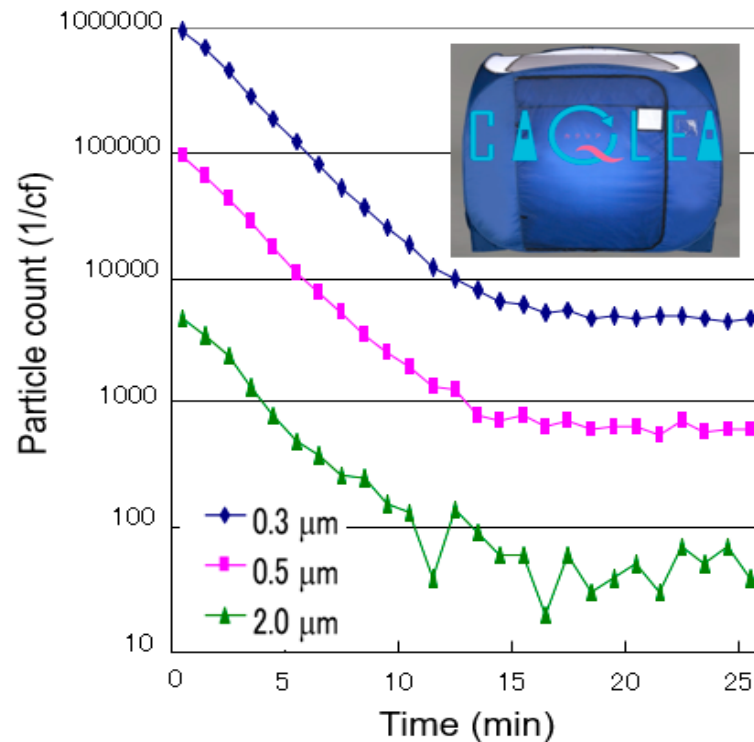

Figure 2. Performance of our new CUSP system, CAQLEA. Shown is the time-dependence of the particle numbers, in CAQLEA, per 1 cubic foot (cf) with diameters of 0.3, 0.5, and 2.0 m.

Figure 3. Clockwise from top left, shown are the outlook of the jump-up CUSP (CAQLEA) system, setup of the experiment seen through the observation window, and the equipment for all-night sleep assessment.

2.1.2. Sleep Assessment in the Jump-Up CUSP (CAQLEA)

In order to demonstrate the applicability of the closed air-flow system of CUSP, we have performed a sleep assessment experiment using the CAQLEA system. The overnight sleep experiment was performed with simultaneous recordings of tiny polysomnography (PSG), an activity watch, and two air-quality sensor modules to estimate sleep quality, metabolism, and body movements when subjects slept in the CAQLEA with gas exchange membrane (GEM).

Due to the jump-up design, the installation process of the CAQLEA can be completed in about 5 min [27]. Developed is an IoT (internet of things) module integrating multiple sensors to wirelessly measure CO_2 concentration, room temperature, humidity, amount of particulate materials with a diameter of 1.0 μm (PM 1.0), 2.5 μm (PM 2.5), and 10 μm (PM 10), and alcohol amount. In this experiment, two modules were utilized to monitor the air quality parameters in the spaces outside and inside the CAQLEA for comparison. In CAQLEA, as shown in Figure 3, the module was placed on a table 15 cm high, and the distance between the module and the subject was near 70 cm to avoid affecting the subject's free movements during sleep. An air cleaner (F-PXM55W, Panasonic Taiwan Co., Ltd., Taipei, Taiwan) was also placed in the CAQLEA to filter out the airborne dusts and microbes (if any) inside. The other sensor module was placed outside the CAQLEA on a table 120 cm high, and the distance between the module and the CAQLEA was 70 cm. The subject mounted the mini polysomnography (PSG) to measure three bipolar physiological signals, including a bipolar electroencephalography [EEG] channel (C3-M2, according to the international 10–20 standard system), a bipolar electrooculography [EOG] channel (positioned 1 cm lateral to the left and right outer the canthi), and a bipolar chin electromyography [EMG] channel with 250 Hz sampling rate and 24-bit resolution. The PSG data were manually scored by a sleep expert following AASM (American Academy of Sleep Medicine) rules [28]. Each 30 s interval (an epoch) was identified as one of the following the sleep stages: wake, N1, N2, N3, and REM. The activity watch would record the subject's wrist acceleration to assess the subject's movement patterns during sleep. The recording experiment started at nearly 00:30 a.m., as the subject's usual on-bed time.

2.1.3. Air Quality Parameters between Outside and Inside of CAQLEA

Figure 4 shows the air quality parameters in the spaces outside and inside the CAQLEA. The source of CO_2 was majorly contributed by the respiration of the subject and may be caused by body movements and metabolism. Therefore, the values of CO_2 concentration in CAQLEA are higher than the measurements outside of the CAQLEA. The trend of CO_2 concentration was gradually decreased due to the gas exchange function of GEM/GEU. For the particulate materials, the amounts of PMs were lower than the resolution of the utilized sensors for most of the recording time in the CAQLEA, and the overnight averages of PMs 1, 2.5, and 10 were 0 ± 0.07, 0.01 ± 0.15 and 0.07 ± 0.36 μg/m^3, respectively. There, values were much lower than the recordings in the outside area of CAQLEA, and it demonstrates the capability of rapidly reaching high cleanliness in a couple of minutes through CUSP–GEU. Regarding humidity, the outside humidity decreased from 53% in the first 30 min to around 49% (overnight average: 49.08 ± 1.07%). The inside humidity fluctuated within the range of 47–52%. These may be caused by the respiration and metabolism of the subject.
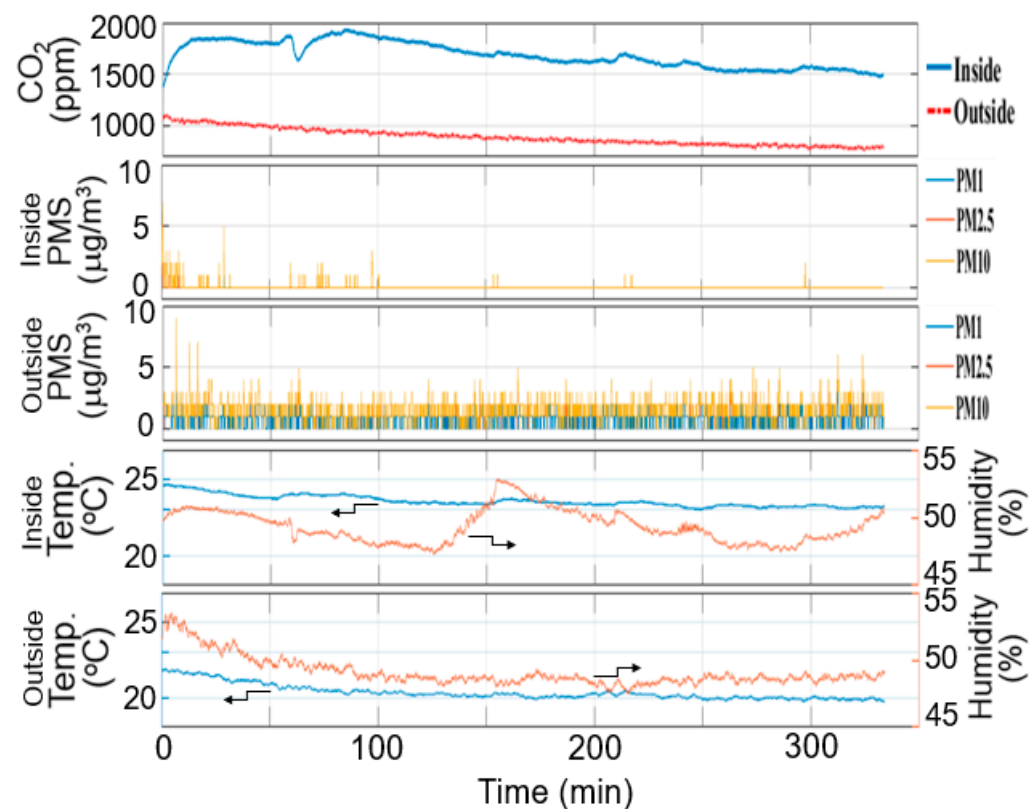
Figure 4. The air quality parameters in the spaces outside and inside the CAQLEA simultaneously measured through two IoT sensor modules.

2.1.4. Sleep Assessment Experiment in CAQLEA

Humans breathe CO_2 out into the surrounding space, and it is the major source in CAQLEA, so we tried to perform non-contact sleep assessment by analyzing the changes in CO_2 concentration. Since the trend of CO_2 concentration was gradually decreased due to the gas exchange function of GEM/GEU, instead of the absolute amount, the standard deviation of CO_2 concentration within 5 min was calculated and used to estimate the sleep patterns. The periods in which the 5 min standard deviation of CO_2 concentration was higher than the threshold are labeled as shown in Figure 5. The all-night sleep stages obtained from manually scoring the PSG recording and the raw data of the activity watch are also included.

In this experiment, the subject stayed 330 min in the CAQLEA overnight. For the sleep parameters, the sleep latency was 12 min, wake after sleep onset time was 45 min, total sleep time was 273 min, and sleep efficiency was 82.73%. The averaged CO_2 standard deviation was 8.65 ppm. There were 4 wake events, and 3 out of there 4 events can be detected by extracting the periods with 5 min standard deviation of CO_2 concentration higher than the threshold (8.65 ppm). The total length of the detected wake events covers 86.5% of the PSG scored wake after sleep onset time (45 min). It can also be observed that large body movements estimated by the activity watch also cause the particles amount changes of PM 10, such as in the four wake events. However, some other non-wake events with body movements also induced amount pulses of PM 10. Therefore, it is feasible to perform non-contact sleep assessments in CAQLEA that can provide high gas exchange and PM-filtering functions. In addition to sleep assessment, more gas sensors could be embedded in the CAQLEA to monitor the metabolic information and respiratory functions for health condition analysis to direct the improvement of quality of life.
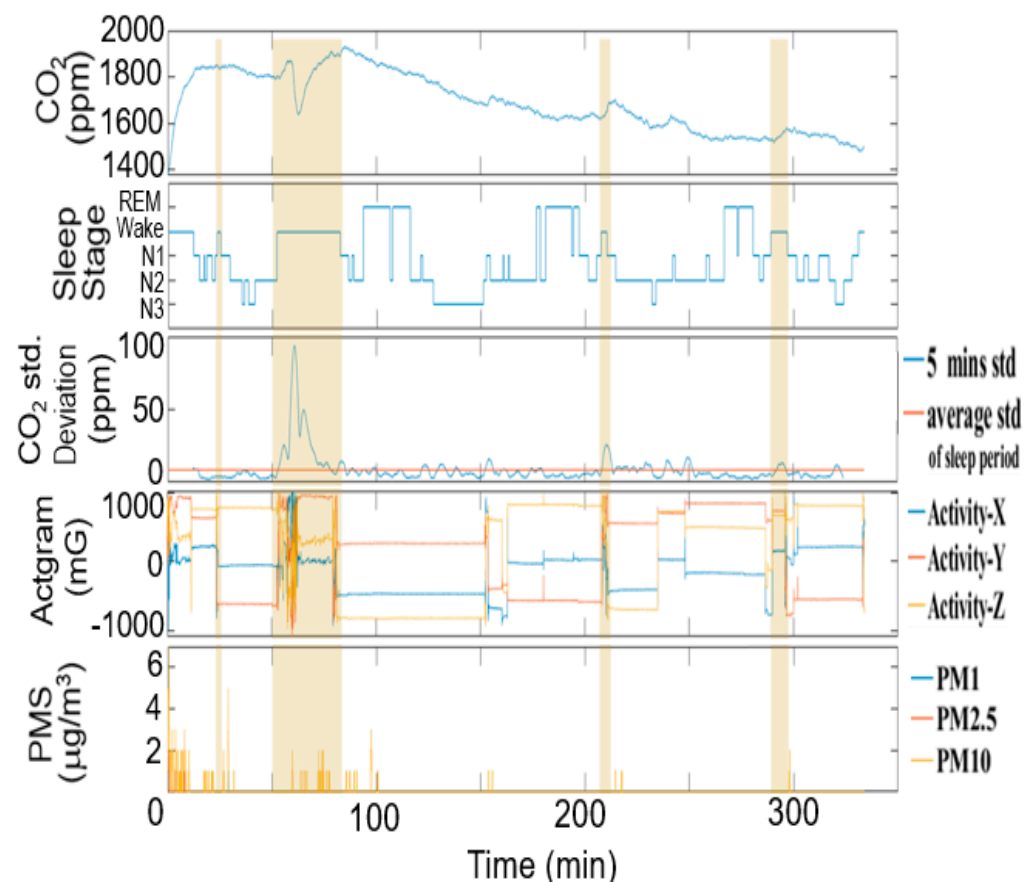
Figure 5. The sleep assessment experiment using the CAQLEA system. The CO_2 concentration, sleep stages obtained from PSG scoring, raw data of the activity watch and amounts of PMs were aligned and compared.

2.2. Designing Solar Power Generation Equipment for CUSP-Based Clean Space

To be employed is 2DPRCS, in which a waveguide having discrete translational symmetries is used, as shown in Figure 1. We call this a discrete-translational-symmetry waveguide (DTSWG) [19,20], which is now shown in detail in Figure 6. In this new structure, the bottom cladding layer, for a 15 μm-thick 2D waveguide (mainstream core), being spatially discontinuous, as shown in the enlarged view at right bottom of Figure 6, gives the 2D waveguide's core an open geometry. Now, the core is connected, through the curved tributary waveguides, to the bottom plane where photons come in vertically, owing to the PDC [13,18]. The thickness of the thin (thick) cladding layer of the curved tributary waveguides is 0.4 μm (1.0 μm), and that of the core layer is 2.66 μm. Thus, the DTSWG is in marked contrast to the conventional waveguides and optical fibers that have continuous translational symmetry. Due to the discrete cladding structure, the waveguide can harvest 3D photons coming vertically from beneath in Figure 6 or, equivalently, at the bottom of Figure 1. At the right end of the WG are placed solar cells or multi-stripe orthogonal photon-photocarrier propagation solar cells (MOP^{3}SC) in which photons propagate in the direction orthogonal to that of the photocarriers [20]. We have performed simulations, in which the core layer with a refractive index of 1.48 depicted in red is sandwiched by the clad layer with a refractive index of 1 depicted in pale blue in Figure 6. DTSWG consists of smoothly connected two partial ellipses: the lower partial ellipse has the role of guiding up-going light to bend, and the upper partial ellipse has the role of enabling smooth propagation of side-going light into the 2D waveguide [13,19]. The height of the vertical lower partial ellipse is 36 μm, and the length of the horizontal upper partial ellipse is about 140 μm. We have calculated optical fields in DTSWG and evaluate the 3D-to-2D conversion efficiency. The optical simulation of light propagation is based on Finite-Difference Time-Domain

(FDTD) method [29]. Note that 3D-to-2D conversion efficiency is calculated by the ratio of the monitor depicted in green to the light intensity at the light source depicted in orange in Figure 6.
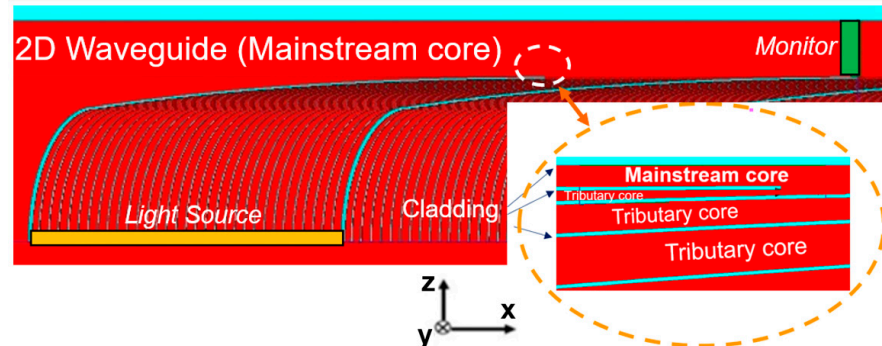

Figure 6. The detailed structure of discrete-translational-symmetry waveguide (DTSWG), overall configuration for which is given in Figure 1. The 2D waveguide (mainstream core) is 15 m thick, the height of the vertical lower partial ellipse is 36 m, and the length of the horizontal upper partial ellipse is about 140 m. The thickness of the thin (thick) cladding layer (pale blue) of the curved tributary waveguides is 0.4 m (1.0 m), and that of the core layer is 2.66 m. The spacing between the thick cladding layer of the curved tributary waveguides is 85 m.

In optical simulations, first, we have used coherent light with various wavelengths as an incoming light and evaluated the 3D-to-2D conversion efficiency of the light. Since the DTSWG is a catoptric system in which the incoming light propagates in core layers with reflections by cladding layers, basically, there should be no wavelength dependence in the 3D-to-2D conversion efficiency. As shown in Figure 7, however, we have found that DTSWG has distinct wavelength dependence for the coherent light as depicted by the black dashed line. There are 8 peaks with a maximum efficiency of 67% from λ = 380 nm to 1600 nm. We have found that these peaks exist according to regularity and are evenly spaced when the reciprocal of the wavelength is taken as the horizontal axis, which indicates that the peaks shown by black dashed lines in Figure 7 are due to resonance between the wavelength and the spatial period of DTSWG. In fact, DTSWG behaves differently for incoherent light. Phase shifter, which has the ability to change the relative phases of the incident light for each core layer, is attached to the light source to produce the partially incoherent light. When the light is injected with less coherency, the wavelength dependence for coherent light becomes weaker, as shown by blue line in Figure 7. The arithmetic mean of the efficiency for wavelengths from λ = 400 nm to 800 nm is 21.0%, which is almost the same as 20.8% for the case of coherent light. Thus, in a rough calculation, the areas enclosed by the two lines and the horizontal axis in Figure 7 are almost equal, again indicating those peaks are due to the resonance. With sunlight being incoherent, such resonance would not be observed in real use, and the average 3D-to-2D conversion efficiency of ~21% could be provided using the present DTSWG structure.

Next, we have investigated the cause of the apparent low 3D-to-2D conversion efficiency of DTSWG. Figure 8b shows the optical field around the connection region of the vertical-lower and the horizontal-upper partial ellipses when the light is injected from the bottom light source, as shown in Figure 6. A closer look of light propagation notifies us that the light does not fully bend at the connection region of the two partial ellipses. From this result, we understand the apparent low 3D-to-2D conversion efficiency is due to the loss of optical field at the connection region. Thus, we have moved the light injection positions into the horizontal upper partial ellipses and checked the light injection efficiency into the 2D waveguide (mainstream). Figure 8a shows those light injection locations A, B, C, and D, which correspond to slots 1–8, 9–16, 17–24, and 25–32, respectively. Slot 1 is the tributary waveguide located at the left end in Figures 6 and 8a. Figure 8c shows incident angle dependence of the efficiency of the light injection into the 2D waveguide with the light

source located at A, B, C, and D (for λ = 1000 nm). Here, the incident angle, θ, is defined as the angle measured from the z-axis in Figure 6 [or Figure 8a]. The injection efficiency of the waveguide reaches its maximum of about 80% for θ around 80° to 86°, almost irrespective of the light source positions. Thus, by optimizing the waveguide structure around the connection region of the two ellipses, we would be able to have higher 3D-to-2D conversion efficiency of photons.
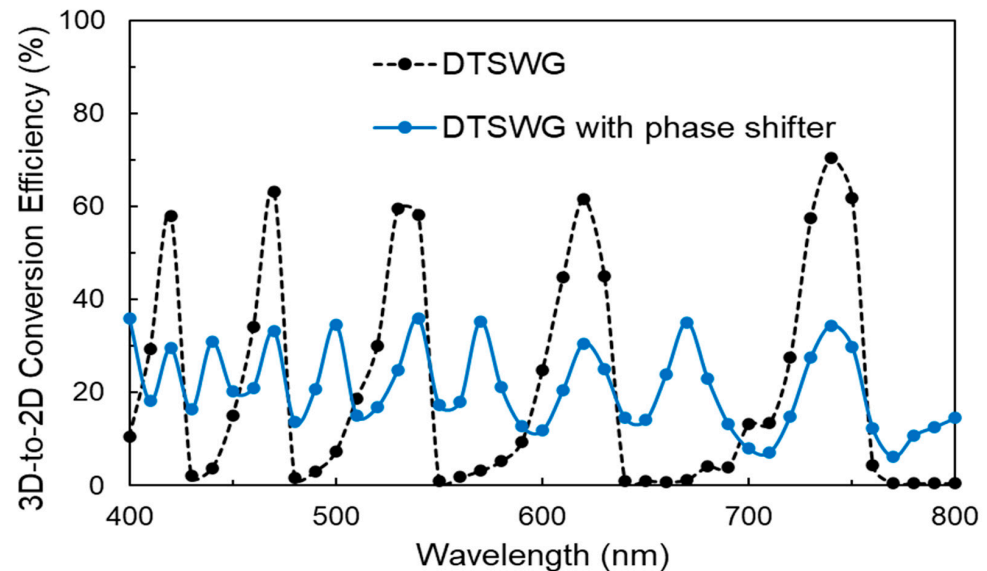

Figure 7. Wavelength dependence of the efficiency of DTSWG and DTSWG with phase shifter.
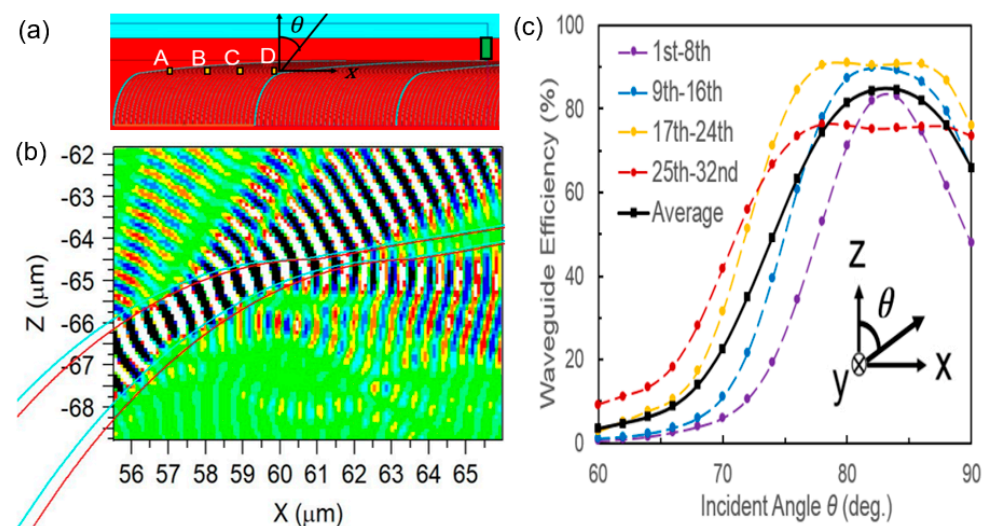

Figure 8. (**a**) Light injection at locations A, B, C, and D in the upper partial ellipses, (**b**) simulation of the optical field at around the connection region of the vertical-lower and the horizontal-upper partial ellipses, and (**c**) incident angle θ dependence of the efficiency of the light injection into the 2D waveguide at locations A, B, C, and D in the upper partial ellipses (for λ = 1000 nm).

3. Discussion

We discuss how we can successfully design and build a system in which medical treatment can be provided with high cleanliness, even in an outdoor environment for injured persons and patients with infectious diseases. If conventional solar cells are put on the surface of a compact clean space set in an outdoor environment, the sunlight is blocked by the solar cells, and part of the electricity has to be wasted by lighting of the

room, which is obviously not a desirable situation at all. In addition, when a type of LSC [10] is used, the inside is filled with red color, which would not be adequate for a rest space for patients. Our DTSWG, made of a transparent waveguide, would be free from the drawbacks of those systems based on conventional technologies. As discussed in the preceding sections, basically, we already have all of the needed elemental technologies to implement those energo-environmental clean systems as depicted in Figure 1, which can be regarded as a miniature system of CUSP-integrated buildings equipped with 2DPRCS [26]. In the following, we will focus on the coupling of 2DPRCS with CUSP. The system would be suitable to provide injured persons or people who have been suffering from disasters such as huge earthquakes with a clean environment in which these people would undergo operations or other medical treatment depending on their health condition. The first step of the application of those clean systems, however, would be to provide these people with a clean space so that they can stay in a clean space free of possible infectious diseases. Such a shelter is actually needed, as we have seen, for example, in New York in 2020 [30]. Also in need is the ability to monitor their health condition or status through the sleep assessment or rest-state assessment, in general, because those functions need less power and are relatively easily implemented.

As for the usage of those nursing rest spaces, because an FFT's power consumption is, for example, as low as 14 W~41 W [31] and GEM/GEU operates based on molecule diffusion using thermal energy kT of the room, we are not in need of heavy electric power if we use the CUSP·GEU-based clean systems. For this system, as seen in Figure 7, the waveguide with present geometry could realize an average waveguiding efficiency of ~20%; with respect to the wavelength, we would be able to generate electricity of $20\% \times (1\,\text{KW}/\text{m}^2 \times 40\%) \times \xi \sim 50\ \text{W}/\text{m}^2$ when we use a tandem solar cell [32] of efficiency 40%, where the coefficient ξ is estimated to be ~0.65, assuming that PDC efficiency is ~70% and reflection of the guided sunlight at the solar-cell surface can be reduced to ~5% using the low reflection technology [33]. So, for this purpose, the 2DPRCS waveguide with an area of ~1 m^2 (~3 m^2 if PDC efficiency is ~20%) is enough to make this energo-environmental clean system work well with a storage battery backup to average the power during the daytime of a sunny day.

In the cross-sectional view at the bottom of Figure 1, we note that the 2DPRCS, realized by a redirection waveguide (RWG) consisting of a photo-propagation direction converter (PDC) and discrete-translational-symmetry waveguide (DTSWG) and a planar (2D) waveguide with a solar-cell at its edge embodies a natural concentrator system in which concentration factor is given by the photo-harvesting area, $L \times D$, divided by the edge light-injection area, $D \times d$, i.e., L/d, with L, D, and d being, respectively, the harvesting length, width, and the 2D planar waveguide thickness that matches the solar-cell's light injection area. Thus, the concentration is with L/d being ~10 cm/100 μm = 1000, typically. Thus, with 2DPRCS, realized is a highly effective concentrator system, as a whole. Since in 2DPRCS, the waveguides, being flexible 2D structures, can be embedded into the surface of the compact CUSP, as shown in the top right inset of Figure 1, high power generation and more power-hungry medical treatment would also become possible.

For applications like those shown in Figure 3, since the total power consumption of those IOT devices is less than 1 W, 2DPRCS waveguide with an area of ~2 m^2 would be safe to secure the operation of the system, even including FFU's power consumption. The shortcomings of our system, so far, are that the current 3D-to-2D conversion efficiency shown in Figure 7 is not high enough when power-hungry processes such as surgery or operation are needed for patients inside the energo-environmental clean system. However, a wider area of 2DPRCS waveguide of ~10 m^2 plus a higher waveguiding efficiency of 80%, as suggested in Figure 8, would be achieved in the near future, and those power-hungry processes could also be provided in the near future. The closed-air-flow system of CUSP·GEU, providing us with a personal clean environment (PCe), would be of increasing importance.

4. Conclusions and Future Outlook

We have considered the energy-related and environmental issues of compact clean systems simultaneously in an interconnected manner. Demonstrated is a versatile closed-air system composed of the clean unit system platform (CUSP) and gas exchange membranes (GEMs). The concentration control of gasses, such as O_2, CO_2, and others, is achieved by the diffusion of molecules through GEM when a concentration gradient exists across GEM, in marked contrast to the conventional open air-flow system in which huge air-flow exists between outside and inside of the room by mechanical ventilation. The CUSP/GEM system lifts off the spatial degeneracy of filtration and ventilation at FFU of conventional systems. A jump-up type of CUSP, called CAQLEA, serves as an excellent platform for sleep assessment and other medical applications. The CUSP/GEM system is a closed air-flow system lifting off the spatial degeneracy of filtration and ventilation at FFU in conventional systems. In the CUSP/GEM system, even a medium-quality, low-power FFU is good enough and quite efficient in reducing airborne dust/microbe density by controlling gas-molecule concentrations for any closed space, including medical systems for treating COVID-19. Owing to the GEU exploiting diffusion process that needs no electricity and the energy-saving FFU, CUSP·GEU system can operate at very low power consumption. The closed air-flow system of CUSP·GEU, providing us with a personal clean environment (PCe), would be the clean system for all of us.

We also have performed optical simulations of discrete-translational-symmetry waveguide (DTSWG), which is necessary to realize a new photovoltaic system of the Two-Dimensional PhotoRecepto-Conversion Scheme (2DPRCS), in which photo-harvesting and photoelectric-conversion part are spatially separated but two-dimensionally connected, lifting off another spatial degeneracy of those functions of photoreception and photoconversion in conventional typical solar cells. By optimizing the waveguide structure, we would be able to have higher 3D-to-2D conversion efficiency of photons. The 2DPRCS frees us from heavy use of semiconductors, and the CUSP/GEU system can take good care of any closed spaces. When degeneracy off-lifting 2DPRCS and CUSP/GEU are combined or cross-linked, we would be able to build a new energo-environmental system not only for medical applications but also for achieving sustainable development goals (SDGs).

References

1. Sze, S.M. Solar cells. In *Physics of Semiconductor Devices*, 2nd ed.; John Wiley & Sons: New York, NY, USA, 1981; pp. 790–838.
2. Ohmi, T. Future trends and applications of ultra-clean technology. In Proceedings of the International Technical Digest on Electron Devices Meeting, Washington, DC, USA, 3–6 December 1989; p. 50.
3. Fumagallia, C.; Zocchi, C.; Tassetti, L.; Silverii, M.V.; Amato, C.; Livi, L.; Giovannoni, L.; Verrillo, F.; Bartoloni, A.; Marcucci, R.; et al. Careggi AOU COVID-19 Follow-up study Group; Factors associated with persistence of symptoms 1 year after COVID-19: A longitudinal, prospective phone-based interview follow-up cohort study. *Eur. J. Intern. Med.* **2022**, *97*, 36–41. [CrossRef] [PubMed]
4. The Bubble Operating Theatre. Available online: https://msf.org.au/sites/default/files/attachments/msf_bubble_operating_theatre.pdf (accessed on 30 December 2022).
5. Hsieh, T.; Liu, Y.; Liang, S.; Yasutake, M.; Ishibashi, A. Tent-type CUSP for Air Cleaning and Non-contact Sleep Assessment. In Proceedings of the 3rd International Conference on Computational Biology and Bioinformatics, ICCBB 2019, Nagoya, Japan, 17–19 October 2019; pp. 47–51.
6. Blanco, M.J.; Ramirez Santigosa, L. (Eds.) *Advances in Concentrating Solar Thermal Research and Technology*; Woodhead Publishing: Soston, UK, 2018. [CrossRef]
7. IBM. Available online: https://arstechnica.com/science/2013/04/ibms-solar-tech-is-80-efficient-thanks-to-supercomputer-know-how/ (accessed on 19 January 2021).
8. Van Sark, W.G.J.H.M.; Barnham, K.W.J.; Slooff, L.H.; Chatten, A.J.; Büchtemann, A.; Meyer, A.; McCormack, S.J.; Koole, R.; Farrell, D.J.; Bose, R.; et al. Luminescent Solar Concentrators—A review of recent results. *Opt. Express* **2013**, *16*, 21773–21792. [CrossRef] [PubMed]
9. Meinardi, F.; Bruni, F.; Brovelli, S. Luminescent solar concentrators for building-integrated photovoltaics. *Nat. Rev. Mater.* **2017**, *2*, 17072. [CrossRef]
10. Corrado, C.; Leow, S.W.; Osborn, M.; Ian Carbone, I.; Hellier, K.; Short, M.; Alers, G.; Carter, S.A. Power generation study of luminescent solar concentrator greenhouse. *J. Renew. Sustain. Energy* **2016**, *8*, 043502. [CrossRef]
11. Jenkins, P.P.; Scheiman, D.A.; Hoheisel, R.; Lorentzen, J.R.; Fischer, R.P.; Wayne, D.T.; Lynn, B.E.; Pogue, C.M.; Jaffe, P. Challenges in receiver design for free-space optical power transfer. In Proceedings of the 1st Optical Wireless and Fiber Power Transmission Conference, OWPT-5-04, Yokohama, Japan, 23–25 April 2019.
12. Masui, Y.; Bricker, D.; Vorontsov, M.A.; Weyrauch, T. Performance analysis of photovoltaic arrays for remote power beaming through the atmosphere. In Proceedings of the 1st Optical Wireless and Fiber Power Transmission Conference, OWPT-9-02, Yokohama, Japan, 23–25 April 2019.
13. Ishibashi, A.; Okura, Y.; Sawamura, N. Lifting Off Spatial Degeneracy of Functions, Where Does It Lead Us for Photovoltaic Device Systems? *Energies* **2020**, *13*, 5234. [CrossRef]
14. Ishibashi, A.; Kasai, T.; Sawamura, N. Tapered Redirection Waveguide in Two Dimensionally connected Photo Recepto Conversion Scheme (2DPRCS). In Proceedings of the 3rd Optical Wireless and Fiber Power Transmission Conference, OWPT-1-03, Yokohama, Japan, 19–21 April 2021.
15. Ishibashi, A.; Kaiju, H.; Yamagata, Y.; Kawaguchi, N. Connected box-units-based compact highly clean environment for cross-disciplinary experiments platform. *Electron. Lett.* **2005**, *41*, 735–736. [CrossRef]
16. Kawaguchi, N.; Rahaman, D.; Kaiju, H.; Ishibashi, A. Physical Analysis of Connected Clean Units in Clean-Unit System Platform. *Jpn. J. Appl. Phys.* **2006**, *45*, 6481–6483. [CrossRef]
17. Rahaman, M.D.; Kaiju, H.; Kawaguchi, N.; Ishibashi, A. Ultra-High Cleanliness of ISO Class Minus 1 Measured in Triply Connected Clean-Unit System Platform. *Jpn. J. Appl. Phys.* **2008**, *47*, 5712–5716. [CrossRef]
18. Ishibashi, A.; Kobayashi, H.; Taniguchi, T.; Kondo, K.; Kasai, T. Optical Simulation for Multi-Striped Orthogonal Photon-Photocarrier-Propagation Solar Cell (MOP^{3}SC) with Redirection Waveguide. *3D Res.* **2016**, *7*, 33. [CrossRef]
19. Ishibashi, A.; Kasai, T.; Sawamura, N. Redirection Waveguide having Discrete Translational Symmetry for Photovoltaic Systems with Solar-Cell Units Placed at the Periphery. *Energies* **2018**, *11*, 3498. [CrossRef]
20. Ishibashi, A.; Sawamura, N.; Matsuoka, T.; Kobayashi, H.; Kasai, T. Asymmetric Waveguide-Coupled Scheme for Multi-striped Orthogonal Photon-Photocarrier Propagation Solar Cell (MOP^{3}SC). *Trans. Mater. Res. Soc. Jpn.* **2019**, *44*, 187–191. [CrossRef]
21. Net Zero-Energy Buildings. Available online: https://en.wikipedia.org/wiki/Zero-energy_building (accessed on 30 December 2022).
22. Ishibashi, A.; Ishibashi, F. Wall, System of Highly Clean Rooms, Production Method Thereof and Construction. U.S. Patent 10,677,483, 9 June 2020.
23. Ishibashi, A.; Yasutake, M.; Ishibashi, F. System and Method Using Information of Involuntary Body Movement during Sleep, and Sleeping State Detection System and Method. U.S. Patent 10,172,547, 8 January 2019.
24. Ishibashi, A.; Noguchi, N.; Etoh, T.; Matsuda, J.; Ohashi, Y. Clean unit system platform (CUSP) based upon 100% feed-back closed-system. In Proceedings of the 35th Annual Technical Meeting on Air Cleaning and Contamination Control, Tokyo, Japan, 24–25 April 2018; pp. 38–41.
25. Ishibashi, A.; Eto, T.; Noguchi, N.; Matsuda, J. Building, and Method for Controlling Gas Molecule Concentration in Living and/or Activity Space in Building. U.S. Patent 11364465, 21 June 2022.

26. Ishibashi, A.; Sawamura, N.; Zhou, Z.; Hong, X.; Wang, X.; Wang, Y.; Kato, N. Lifting off spatial functional degeneracies in solar cells and clean rooms, where does it lead us for mitigating climate change in cities? In Proceedings of the 4th Optical Wireless and Fiber Power Transmission Conference, OWPT2022, Yokohama, Japan, 18–21 April 2022.
27. CAQLEA. Available online: https://caqlea.com/ (accessed on 16 November 2022).
28. American Academy of Sleep Medicine. Available online: https://aasm.org/ (accessed on 17 November 2022).
29. FullWAVE. Available online: https://www.synopsys.com/photonic-solutions/rsoft-photonic-device-tools/passive-device-fullwave.html (accessed on 30 December 2022).
30. BBC News Japan. Available online: https://www.bbc.com/japanese/features-and-analysis-52087717 (accessed on 30 December 2022).
31. Air Cleaner (See for Example). Available online: https://kadenfan.hitachi.co.jp/support/airclean/item/EP-Z30R/manual.html (accessed on 30 December 2022).
32. Geisz, J.F.; France, R.M.; Schulte, K.L.; Steiner, M.A.; Norman, A.G.; Guthre, H.L.; Young, M.R.; Song, T.; Moriarty, T. Six-junction III–V solar cells with 47.1% conversion efficiency under 143 suns concentration. *Nat. Energy* **2020**, *5*, 326–335. [CrossRef]
33. Irishika, D.; Imamura, K.; Kobayashi, H. Ultralow reflectivity surfaces by formation of nanocrystalline Si layer for crystalline Si solar cells. *Sol. Energy Mater. Sol. Cells* **2015**, *141*, 1–6. [CrossRef]